

# LAGRANGIAN MESHFREE FORMULATION FOR ANALYSIS OF GEOTECHNICAL MATERIALS

By Cheng-Tang Wu,<sup>1</sup> Jiun-Shyan Chen,<sup>2</sup> Liqun Chi,<sup>3</sup> and Frank Huck<sup>4</sup>

**ABSTRACT:** A Lagrangian reproducing kernel formulation is introduced as an approximation of field variables under the Galerkin meshfree framework of geomechanics. The reproducing kernel approximation is formulated with reference to the material coordinates, yielding an approach that is applicable to both total and updated Lagrangian formulations. In the method presented, geotechnical materials described by pressure-sensitive multisurface plasticity with a cap hardening rule are considered in the meshfree formulation. The solution obtained from the meshfree method with linear basis was compared to that of bilinear finite elements for elastoplastic analysis of geotechnical materials.

## INTRODUCTION

Recent developments in meshfree methods add an additional dimension to computational mechanics (Monaghan 1988; Nayroles et al. 1992; Belytschko et al. 1994, 1996; Sulsky et al. 1994; Liu et al. 1995a,b; Chen et al. 1996; Duarte and Oden, 1996; Melenk and Babuska 1996; Randles and Libersky 1996; Atluri and Zhu 1998). The commonly used approximation methods in meshfree formulation are the moving least-squares approximation (Lancaster et al. 1980; Belytschko et al. 1994), partition of unity (Babuska and Melenk 1997), and the reproducing kernel approximation (Liu et al. 1995). These methods do not rely on the conventional grid approach to define approximation functions. Several recent advances have been made to enhance the computational efficiency of meshfree methods, for example, enhanced imposition of boundary conditions (Gunther et al. 1997; Kaljevic and Saigal 1997; Chen et al. 1998; Chen and Wang 2000a), and stabilized nodal integration methods (Beissel and Belytschko 1996; Chen et al. 2001b). In comparison with conventional finite-element methods, the characteristics of naturally conforming, exemption from meshing, and higher convergence rate make meshfree methods attractive alternative numerical techniques for analysis of geotechnical materials.

Lagrangian meshfree methods for history-independent and -dependent materials have been developed for large deformation and contact problems (Chen et al. 1996, 1998; Chen and Wang 2000a). For nonlinear elasticity problems, the material derivatives can be obtained by direct differentiation, since stress and strain measures are referenced to the material coordinate. For inelastic materials, however, a spatial derivative on the Lagrangian shape function requires an additional computation to invert the deformation gradient. It has also been shown (Chen et al. 1998) that using meshfree shape functions referenced to the current configuration, an additional convective transport term must be included in the material time derivatives of field variables involved in the conservation equations.

In this paper, the Lagrangian meshfree formulation is applied to multisurface plasticity for geotechnical applications. A Lagrangian kernel function formulated in a material coordinate is introduced, with reproducing conditions imposed in the material coordinate to construct the Lagrangian meshfree shape functions. The compact support of Lagrangian meshfree shape function covers the same set of material points; therefore, no convective transport effect is required in the formulation. Using this approach, each material point in the space is covered by the same set of meshfree shape functions. This property is important to assure kernel stability in the meshfree analysis of large deformation problems. The weak forms are transformed to the initial configuration, and the unknown field variables are approximated by the Lagrangian meshfree shape functions. For application to geomechanics, a soil-cap model (Mizuno and Chen 1980, 1983; Simo et al. 1988a; Hofstetter et al. 1993) is implemented in the Lagrangian meshfree formulation.

The remainder of the paper is organized as follows. An overview of governing equations for the soil-cap model is given in the next section. The reproducing kernel approximation and construction of meshfree shape functions are presented in the following section. The subsequent section discusses the meshfree formulation and the associated numerical algorithms for geomechanics. Three example problems that examine the performance of the proposed method are analyzed in the penultimate section, with conclusions being presented in the final section.

## GOVERNING EQUATIONS

### Soil-Cap Model

A commonly used two-invariant elliptic cap model originally developed by DiMaggio and Sandler (1971), formulated

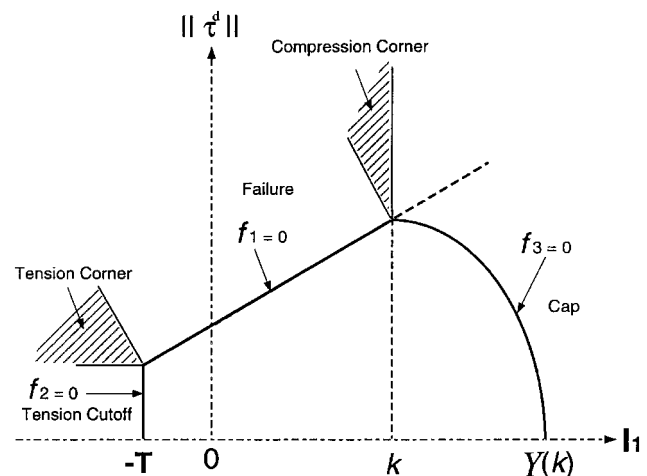


FIG. 1. Soil-Cap Model

<sup>1</sup>Postdoctoral Assoc., Dept. of Mech. Engrg. and Ctr. for Comp.-Aided Des., Univ. of Iowa, Iowa City, IA 52242-1527.

<sup>2</sup>Assoc. Prof., Dept. of Mech. Engrg. and Ctr. for Comp.-Aided Des., Univ. of Iowa, Iowa City, IA 52242-1527 (corresponding author). E-mail: jschen@icaen.uiowa.edu

<sup>3</sup>Proj. Engr., Peoria Proving Ground, Caterpillar, Inc., Peoria, IL 61656-1895.

<sup>4</sup>Sr. Proj. Engr., Peoria Proving Ground, Caterpillar, Inc., Peoria, IL 61656-1895.

Note. Associate Editor: Jacob Fish. Discussion open until October 1, 2001. To extend the closing date one month, a written request must be filed with the ASCE Manager of Journals. The manuscript for this paper was submitted for review and possible publication on April 11, 2000; revised November 14, 2000. This paper is part of the *Journal of Engineering Mechanics*, Vol. 127, No. 5, May, 2001. ©ASCE, ISSN 0733-9399/01/0005-0440-0449/\$8.00 + \$.50 per page. Paper No. 22283.

within a framework of associative multisurface plasticity theory is employed as the constitutive model of geotechnical materials herein. This soil-cap constitutive model is defined by a convex yield surface consisting of a failure envelope, an elliptical cap, and a tension cutoff region, as shown in Fig. 1. The three yield surfaces are given as follows:

Shear failure surface: Drucker-Prager yield function

$$f_1(\tau) = \|\tau^d\| - F_e(I_1) \quad \text{for } T \leq I_1 \leq k \quad (1)$$

$$F_e(I_1) = A + BI_1 \quad (2)$$

Tension cutoff surface

$$f_2(\tau) = I_1 - T \quad (3)$$

Ellipsoidal cap

$$f_3(\tau, k) = F_c(\tau^d, I_1, k) - F_c(k)^2 \quad \text{for } k \leq I_1 \leq Y(k) \quad (4)$$

$$F_c(\tau, I_1, k) = \sqrt{\|\tau^d\|^2 + \frac{1}{R^2} (I_1 - k)^2} \quad (5)$$

where  $I_1$  = first invariant of the Cauchy stress  $\tau$ ;  $\tau^d$  = deviatoric part of the Cauchy stress;  $A$  and  $B$  = parameters defining the position and slope of the shear failure surface;  $T = I_1$  value at the tension cutoff location;  $R$  = aspect ratio of the ellipsoidal cap;  $k$  determines the interaction point between shear failure surface and the ellipsoidal cap; and  $Y(k)$  = point of interaction between the ellipsoidal cap and the  $I_1$ -axis and is therefore a function of  $k$ . Following the standard conventions of soil mechanics,  $I_1$  is defined as positive for compression. The parameter  $k$  is associated with the strain hardening of volumetric plastic deformation, and also defines the center location of the ellipsoidal cap.

In this cap model, the failure surface passes through the peak point at which the tangent to the cap is horizontal. It should be noted that the yield function is written in a square form that differs from some other formulations (DiMaggio and Sandler 1971; Hofstetter et al. 1993). This form does not affect the consistency condition, but it can generate an efficient formulation for deriving the return mapping algorithm and obtaining the explicit elastoplastic-consistent tangent modulus for small deformation (Wu 1999). Perfect plastic behavior is assumed in the shear failure and tension cutoff yield surfaces. A cap hardening rule that describes the dilatancy and plastic compaction of geotechnical materials is employed

$$\varepsilon_v^p = W[1 - e^{-\alpha Y(k)}] \quad (6)$$

where  $\varepsilon_v^p$  = volumetric plastic strain; and  $W$  and  $\alpha$  are material parameters. Several assumptions are made regarding the constitutive model: (1) following Sandler and Rubin (1979), the movement of the cap is prevented when the stress point is at the compression corner; (2) the cap is exempted from retraction (Sandler and Rubin 1979); and (3) if  $k < 0$ , then set  $k = 0$  (Sandler and Rubin 1979).

The associative flow rule for multisurface plasticity is formulated according to Koiter's (1953) generalization

$$\dot{\varepsilon}^p = \sum_{i=1}^3 \dot{\gamma}_i \frac{\partial f_i}{\partial \tau} \quad (7)$$

where  $\varepsilon^p$  = plastic strain; and  $\dot{\gamma}_i$ ,  $i = 1, 2, 3$  = plastic consistency parameters associated with the three yield surfaces.

## Lagrangian Strong and Weak Forms

In a Lagrangian formulation, the motion of all the material particles in the body is followed from the initial configuration  $\Omega_X$  with boundary  $\Gamma_X$  to the current configuration  $\Omega_x$  with boundary  $\Gamma_x$ . The motion of a material particle originally lo-

cated at a position  $\mathbf{X} \in \Omega_X$  is described by mapping  $\mathbf{x} = \varphi(\mathbf{X}, t)$  ( $x_i = \varphi_i(\mathbf{X}, t)$ ), where  $\mathbf{x} \in \Omega_x$  is the spatial location of the material particle  $\mathbf{X}$  at time  $t$ , and  $\varphi_i$  is the mapping function. The material displacement is defined by

$$\mathbf{u}(\mathbf{X}, t) = \varphi(\mathbf{X}, t) - \mathbf{X} \quad (8)$$

For history-dependent materials, the constitutive equations are expressed in the current configuration, therefore it is more convenient to reference the kinematic and kinetic variables to the current configuration in the variational equation. The following boundary-value problem is considered.

Given the body force  $\mathbf{b}$  in the domain  $\Omega_x$ , the surface traction  $\mathbf{h}$  on the natural boundary  $\Gamma_x^{h_i}$ , the prescribed boundary displacement  $g_i$  on the essential boundary  $\Gamma_x^{g_i}$ ,  $\Gamma_x^{g_i} \cup \Gamma_x^{h_i} = \Gamma_x$ , find  $\mathbf{u}$ , such that the following equation is satisfied:

$$\tau_{ij,j} + b_i = 0 \quad \text{in } \Omega_x \quad (9)$$

$$\dot{\tau}_{ij} = C_{ijkl}\dot{u}_{(k,l)} + S_{ijkl}\dot{u}_{[k,l]} \quad \text{in } \Omega_x \quad (10)$$

$$\tau_{ij}n_j = h_i \quad \text{on } \Gamma_x^{h_i} \quad (11)$$

$$u_i = g_i \quad \text{on } \Gamma_x^{g_i} \quad (12)$$

$$u_{(i,j)} = \frac{1}{2}(u_{i,j} + u_{j,i}) \quad \text{in } \Omega_x \quad (13)$$

$$u_{[i,j]} = \frac{1}{2}(u_{i,j} - u_{j,i}) \quad \text{in } \Omega_x \quad (14)$$

where  $\tau$  = Cauchy stress;  $\mathbf{n}$  = unit surface normal of the deformed body;  $f_{,i} \equiv \partial f / \partial x_i$  = spatial derivative;  $C_{ijkl}$  = material-dependent corotational response tensor; and  $S_{ijkl}$  is responsible for the pure rotation of the Cauchy stress rate

$$S_{ijkl} = \frac{1}{2}(\tau_{ij}\delta_{kl} + \tau_{il}\delta_{jk} - \tau_{ik}\delta_{jl} - \tau_{jk}\delta_{il}) \quad (15)$$

The corotational material response tensor  $C_{ijkl}$  associated with the cap model described in the first section can be found in Wu (1999), and is included in the appendix.

The weak form statement of the boundary value problem is to find  $\mathbf{u} \in H_g^1$  ( $H_g^1 = \{\mathbf{u}; \mathbf{u} \in H^1, u_i = g_i \text{ on } \Gamma_x^{g_i}\}$ ), such that for all  $\delta \mathbf{u} \in H_0^1$  ( $H_0^1 = \{\mathbf{w}; \mathbf{w} \in H^1, w_i = 0 \text{ on } \Gamma_x^{g_i}\}$ ), the following equation is satisfied:

$$\int_{\Omega_x} \delta u_{i,j} \tau_{ij} d\Omega - \int_{\Omega_x} \delta u_i b_i d\Omega - \int_{\Gamma_x^{h_i}} \delta u_i h_i d\Gamma = 0 \quad (16)$$

The corresponding incremental equation for the iterative solution procedure is

$$\int_{\Omega_x} \delta u_{i,j} (D_{ijkl} + T_{ijkl}) \Delta u_{k,l} d\Omega_x = r \quad (17)$$

where

$$D_{ijkl} = C_{ijkl} + \tau_{ij}\delta_{kl} - \left( \frac{1}{2}\tau_{il}\delta_{jk} + \frac{1}{2}\tau_{jl}\delta_{ik} + \frac{1}{2}\tau_{ik}\delta_{jl} + \frac{1}{2}\tau_{jk}\delta_{il} \right) \quad (18)$$

$$T_{ijkl} = \tau_{jl}\delta_{ik} \quad (19)$$

and  $r$  emerges from an imbalance of the resultant force. Eqs. (16)–(19) are also referred to as the updated Lagrangian formulation.

## MESHFREE APPROXIMATION

In this research, solution of the governing equations using meshfree approximation is achieved under the framework of the Galerkin method. Several approximation theories can be used to construct meshfree shape functions without reference

to local mesh and node connectivity. Without loss of generality, a reproducing kernel approximation is employed. In this section, the general notations  $\mathbf{x}$  and  $\Omega$  are used to respectively denote the spatial coordinate and problem domain without distinguishing initial and current configurations.

### Continuous Reproducing Kernel Approximation

The reproducing kernel approximation of a function  $v(\mathbf{x})$  begins with the following (Liu et al. 1995):

$$v^R(\mathbf{x}) = \int_{\Omega} v(\mathbf{s}) \bar{\Phi}_a^{[n]}(\mathbf{x}; \mathbf{x} - \mathbf{s}) ds \quad (20)$$

where  $\mathbf{x} \equiv (x_1, x_2, x_3)$ ;  $\mathbf{s} \equiv (s_1, s_2, s_3)$ ;  $ds \equiv ds_1 ds_2 ds_3$ ;  $\mathbf{x} - \mathbf{s} \equiv (x_1 - s_1, x_2 - s_2, x_3 - s_3)$ ;  $\Omega$  = domain of approximation;  $v^R(\mathbf{x})$  = reproduced function of  $v(\mathbf{x})$ ; and  $\bar{\Phi}_a^{[n]}(\mathbf{x}; \mathbf{x} - \mathbf{s})$  = reproducing kernel of degree  $n$  having a compact support measured by dilation parameter  $a$ . The  $n$ th order completeness of reproducing kernel approximation in (20) requires the exact reproduction of the  $n$ th order monomials, i.e.,

$$\int_{\Omega} s_1^i s_2^j s_3^k \bar{\Phi}_a^{[n]}(\mathbf{x}; \mathbf{x} - \mathbf{s}) ds = x_1^i x_2^j x_3^k \text{ for } 0 \leq (i + j + k) \leq n \quad (21)$$

Eq. (21) can be rewritten as

$$\int_{\Omega} (x_1 - s_1)^i (x_2 - s_2)^j (x_3 - s_3)^k \bar{\Phi}_a^{[n]}(\mathbf{x}; \mathbf{x} - \mathbf{s}) ds = \delta_{i0} \delta_{j0} \delta_{k0} \quad (22)$$

for  $0 \leq (i + j + k) \leq n$

Eq. (21) is also referred to as the  $n$ th order completeness of the approximation. One way to construct a reproducing kernel  $\bar{\Phi}_a^{[n]}(\mathbf{x}; \mathbf{x} - \mathbf{s})$  to satisfy (22) is to express  $\bar{\Phi}_a^{[n]}(\mathbf{x}; \mathbf{x} - \mathbf{s})$  as

$$\bar{\Phi}_a^{[n]}(\mathbf{x}; \mathbf{x} - \mathbf{s}) = C^{[n]}(\mathbf{x}; \mathbf{x} - \mathbf{s}) \Phi_a(\mathbf{x} - \mathbf{s}) \quad (23)$$

where  $\Phi_a(\mathbf{x} - \mathbf{s})$  = kernel function that defines the smoothness of the approximation with compact support measure  $a$ ; and  $C^{[n]}(\mathbf{x}; \mathbf{x} - \mathbf{s})$  = correction function that defines the order of completeness in the approximation. To meet the requirement in (22), the correction function is expressed as a linear combination of a set of complete  $n$ th order monomial basis functions  $\{1, (x_1 - s_1), (x_2 - s_2), (x_3 - s_3), (x_1 - s_1)^2, \dots, (x_3 - s_3)^n\}$

$$C^{[n]}(\mathbf{x}; \mathbf{x} - \mathbf{s}) = \sum_{i+j+k=0}^n (x_1 - s_1)^i (x_2 - s_2)^j (x_3 - s_3)^k b_{ijk}(\mathbf{x}) = \mathbf{H}^{[n]T}(\mathbf{x} - \mathbf{s}) \mathbf{b}(\mathbf{x}) \quad (24)$$

where

$$\mathbf{H}^{[n]T}(\mathbf{x} - \mathbf{s}) = [1, (x_1 - s_1), (x_2 - s_2), (x_3 - s_3), (x_1 - s_1)^2, \dots, (x_3 - s_3)^n] \quad (25)$$

$$\mathbf{b}^T(\mathbf{x}) = [b_{000}(\mathbf{x}), b_{100}(\mathbf{x}), b_{010}(\mathbf{x}), b_{001}(\mathbf{x}), b_{200}(\mathbf{x}), \dots, b_{00n}(\mathbf{x})] \quad (26)$$

Note that in the reproducing kernel approximation, the coefficients  $b_{ijk}(\mathbf{x})$  are allowed to be functions of  $\mathbf{x}$ . The coefficients  $b_{ijk}(\mathbf{x})$  can be determined by introducing a Taylor series expansion of  $v(\mathbf{x})$  into (20) and imposing exact reproduction of the monomials. Here we consider a simple procedure by substituting (23) and (24) into (22) to yield

$$\left[ \int_{\Omega} (x_1 - s_1)^i (x_2 - s_2)^j (x_3 - s_3)^k \mathbf{H}^{[n]T}(\mathbf{x} - \mathbf{s}) \Phi_a(\mathbf{x} - \mathbf{s}) ds \right] \mathbf{b}(\mathbf{x}) = \delta_{i0} \delta_{j0} \delta_{k0} \text{ for } 0 \leq (i + j + k) \leq n \quad (27)$$

Subsequently, (27) can be rewritten as

$$\left[ \int_{\Omega} \mathbf{H}^{[n]}(\mathbf{x} - \mathbf{s}) \mathbf{H}^{[n]T}(\mathbf{x} - \mathbf{s}) \Phi_a(\mathbf{x} - \mathbf{s}) ds \right] \mathbf{b}(\mathbf{x}) = \mathbf{H}^{[n]}(\mathbf{0}) \quad (28)$$

or

$$\mathbf{M}^{[n]}(\mathbf{x}) \mathbf{b}(\mathbf{x}) = \mathbf{H}^{[n]}(\mathbf{0}) \quad (29)$$

where

$$\mathbf{M}^{[n]}(\mathbf{x}) = \int_{\Omega} \mathbf{H}^{[n]}(\mathbf{x} - \mathbf{s}) \mathbf{H}^{[n]T}(\mathbf{x} - \mathbf{s}) \Phi_a(\mathbf{x} - \mathbf{s}) ds \quad (30)$$

$$\mathbf{H}^{[n]T}(\mathbf{0}) = [1, 0, \dots, 0] \quad (31)$$

and  $\mathbf{M}^{[n]}$  =  $n$ th order moment matrix of  $\Phi_a$ . Substituting the coefficient vector  $\mathbf{b}(\mathbf{x})$  from (29) into (23), the following  $n$ th reproducing kernel function can be obtained:

$$\bar{\Phi}_a^{[n]}(\mathbf{x}; \mathbf{x} - \mathbf{s}) = \mathbf{H}^{[n]T}(\mathbf{0}) \mathbf{M}^{[n]-1}(\mathbf{x}) \mathbf{H}^{[n]}(\mathbf{x} - \mathbf{s}) \Phi_a(\mathbf{x} - \mathbf{s}) \quad (32)$$

### Discrete Reproducing Kernel Approximation

A discrete counterpart of the continuous reproducing kernel approximation of (20) can be written as

$$v^h(\mathbf{x}) = \sum_{I=1}^{NP} \bar{\Phi}_a^{[n]}(\mathbf{x}; \mathbf{x} - \mathbf{x}_I) v_I \quad (33)$$

where  $\mathbf{x}_I$ ,  $I = 1, NP$  = position vectors of a set of discrete points in the domain  $\Omega$ ;  $NP$  = number of discrete points;  $\bar{\Phi}_a^{[n]}(\mathbf{x}; \mathbf{x} - \mathbf{x}_I)$  =  $n$ th order reproducing kernel centered at location  $\mathbf{x}_I$ , and the  $v_I$  = coefficients of approximation. For  $n$ th order completeness,  $\bar{\Phi}_a^{[n]}(\mathbf{x}; \mathbf{x} - \mathbf{x}_I)$  must satisfy the discrete reproducing conditions

$$\sum_{I=1}^{NP} x_1^i x_2^j x_3^k \bar{\Phi}_a^{[n]}(\mathbf{x}; \mathbf{x} - \mathbf{x}_I) = x_1^i x_2^j x_3^k \text{ for } 0 \leq (i + j + k) \leq n \quad (34)$$

or

$$\sum_{I=1}^{NP} (x_1 - x_{1I})^i (x_2 - x_{2I})^j (x_3 - x_{3I})^k \bar{\Phi}_a^{[n]}(\mathbf{x}; \mathbf{x} - \mathbf{x}_I) = \delta_{i0} \delta_{j0} \delta_{k0} \text{ for } 0 \leq (i + j + k) \leq n \quad (35)$$

To meet the discrete reproducing conditions in (34),  $\bar{\Phi}_a^{[n]}(\mathbf{x}; \mathbf{x} - \mathbf{x}_I)$  can be constructed similar to (24) using

$$\bar{\Phi}_a^{[n]}(\mathbf{x}; \mathbf{x} - \mathbf{x}_I) = C^{[n]}(\mathbf{x}; \mathbf{x} - \mathbf{x}_I) \Phi_a(\mathbf{x} - \mathbf{x}_I) \quad (36)$$

where

$$C^{[n]}(\mathbf{x}; \mathbf{x} - \mathbf{x}_I) = \sum_{i+j+k=0}^n (x_1 - x_{1I})^i (x_2 - x_{2I})^j (x_3 - x_{3I})^k b_{ijk}(\mathbf{x}) = \mathbf{H}^{[n]T}(\mathbf{x} - \mathbf{x}_I) \mathbf{b}(\mathbf{x}) \quad (37)$$

Substituting (36) into (35) yields

$$\left[ \sum_{I=1}^{NP} (x_1 - x_{1I})^i (x_2 - x_{2I})^j (x_3 - x_{3I})^k b_{ijk}(\mathbf{x}) \mathbf{H}^{[n]T}(\mathbf{x} - \mathbf{x}_I) \cdot \Phi_a^{[n]}(\mathbf{x}; \mathbf{x} - \mathbf{x}_I) \right] \mathbf{b}(\mathbf{x}) = \delta_{i0} \delta_{j0} \delta_{k0} \text{ for } 0 \leq (i + j + k) \leq n \quad (38)$$

or

$$\left[ \sum_{I=1}^{NP} \mathbf{H}^{[n]}(\mathbf{x} - \mathbf{x}_I) \mathbf{H}^{[n]T}(\mathbf{x} - \mathbf{x}_I) \Phi_a^{[n]}(\mathbf{x}; \mathbf{x} - \mathbf{x}_I) \right] \mathbf{b}(\mathbf{x}) = \mathbf{H}^{[n]}(\mathbf{0}) \quad (39)$$

Further substitution of the coefficient vector  $\mathbf{b}(\mathbf{x})$  from (39) into (36) yields the discrete  $n$ th order reproducing kernel

$$\bar{\Phi}_a^{[n]}(\mathbf{x}; \mathbf{x} - \mathbf{x}_I) = \mathbf{H}^{[n]T}(\mathbf{0}) \mathbf{M}^{[n-1]}(\mathbf{x}) \mathbf{H}^{[n]}(\mathbf{x} - \mathbf{x}_I) \Phi_a(\mathbf{x} - \mathbf{x}_I) \quad (40)$$

where

$$\mathbf{M}^{[n]}(\mathbf{x}) = \sum_{I=1}^{NP} \mathbf{H}^{[n]}(\mathbf{x} - \mathbf{x}_I) \mathbf{H}^{[n]T}(\mathbf{x} - \mathbf{x}_I) \Phi_a(\mathbf{x} - \mathbf{x}_I) \quad (41)$$

Hence, the discrete reproducing kernel approximation is now expressed by

$$\begin{aligned} v^h(\mathbf{x}) &= \sum_{I=1}^{NP} \mathbf{H}^{[n]T}(\mathbf{0}) \mathbf{M}^{[n-1]}(\mathbf{x}) \mathbf{H}^{[n]}(\mathbf{x} - \mathbf{x}_I) \bar{\Phi}_a(\mathbf{x} - \mathbf{x}_I) v_I \\ &\equiv \sum_{I=1}^{NP} \Psi_I^{[n]}(\mathbf{x}) v_I \end{aligned} \quad (42)$$

where

$$\begin{aligned} \Psi_I^{[n]}(\mathbf{x}) &= \bar{\Phi}_a^{[n]}(\mathbf{x}; \mathbf{x} - \mathbf{x}_I) \\ &= \mathbf{H}^{[n]T}(\mathbf{0}) \mathbf{M}^{[n-1]}(\mathbf{x}) \mathbf{H}^{[n]}(\mathbf{x} - \mathbf{x}_I) \Phi_a(\mathbf{x} - \mathbf{x}_I) \end{aligned} \quad (43)$$

The function  $\Psi_I^{[n]}(\mathbf{x})$  will be used as the shape function in the meshfree Galerkin approximation. The smoothness of  $\Psi_I^{[n]}(\mathbf{x})$  is determined by the smoothness of the kernel function  $\Phi_a(\mathbf{x} - \mathbf{x}_I)$ . It should be noted that, in general,  $\Psi_I^{[n]}(\mathbf{x}_I) \neq \delta_{IJ}$ , therefore  $v_I \neq v^h(\mathbf{x}_I)$ . However, if  $\Phi_a(\mathbf{x} - \mathbf{x}_I)$  is singular at  $\mathbf{x} = \mathbf{x}_I$ , it can be shown that  $\Psi_I^{[n]}(\mathbf{x}_I) = 1$ ,  $\Psi_J^{[n]}(\mathbf{x}_I) = 0$ , and  $v_I = v^h(\mathbf{x}_I)$ . Whereas at other nonsingular points  $J$ ,  $\Psi_I^{[n]}(\mathbf{x}_J) \neq 1$ ,  $\Psi_J^{[n]}(\mathbf{x}_J) \neq 0$ , and  $v_J \neq v^h(\mathbf{x}_J)$  (Chen and Wang 2000a). When singularity is introduced to  $\Phi_a(\mathbf{x} - \mathbf{x}_I)$  at all discrete points, then  $\Psi_I^{[n]}(\mathbf{x}_I) = \delta_{IJ}$  and  $v_I = v^h(\mathbf{x}_I)$ .

## LAGRANGIAN MESHFREE DISCRETIZATION

### Lagrangian Shape Functions

In Lagrangian formulation, material behavior is described by tracing the same material point at any time  $t$ ,  $\mathbf{x} = \varphi(\mathbf{X}, t)$ , throughout the history of the deformation. Consequently, with meshfree discretization, discrete points that carry the primary unknown variables are attached to the same set of material points throughout the course of the deformation. With this consideration, the material displacements are approximated using the Lagrangian meshfree shape functions (Chen et al. 1998) as

$$u_i^h(\mathbf{X}, t) = x_i^h(\mathbf{X}, t) - X_i = \sum_{I=1}^{NP} \Psi_I^{[n]}(\mathbf{X}) d_{iI}(t) \quad (44)$$

where  $u_i^h(\mathbf{X}, t) =$  meshfree approximation of  $u_i(\mathbf{X}, t)$ . In this approximation, the meshfree shape functions are constructed independent of history; the history-dependency of the approximation is inherent in the coefficients  $d_{iI}(t)$ . A Lagrangian reproducing condition of the reproducing kernel approximation is then introduced as

$$\sum_{I=1}^{NP} X_1^i X_2^j X_3^k \Psi_I^{[n]}(\mathbf{X}) = X_1^i X_2^j X_3^k \text{ for } 0 \leq (i + j + k) \leq n \quad (45)$$

To meet the Lagrangian reproducing condition in (45), the meshfree shape function is expressed in the following form:

$$\Psi_I^{[n]}(\mathbf{X}) = C^{[n]}(\mathbf{X}; \mathbf{X} - \mathbf{X}_I) \Phi_a(\mathbf{X} - \mathbf{X}_I) \quad (46)$$

where

$$\begin{aligned} C^{[n]}(\mathbf{X}; \mathbf{X} - \mathbf{X}_I) &= \sum_{i+j+k=0}^{NP} (X_1 - X_{1I})^i (X_2 - X_{2I})^j (X_3 - X_{3I})^k b_{ijk}(\mathbf{X}) \\ &= \mathbf{H}^{[n]T}(\mathbf{X} - \mathbf{X}_I) \mathbf{b}(\mathbf{X}) \end{aligned} \quad (47)$$

Following the same procedures described in the third section, the coefficient vector  $\mathbf{b}(\mathbf{X})$  is solved by substituting (46) and (47) into (45), yielding the Lagrangian shape function

$$\Psi_I^{[n]}(\mathbf{X}) = \mathbf{H}^{[n]T}(\mathbf{0}) \mathbf{M}^{[n-1]}(\mathbf{X}) \mathbf{H}^{[n]}(\mathbf{X} - \mathbf{X}_I) \Phi_a(\mathbf{X} - \mathbf{X}_I) \quad (48)$$

$$\mathbf{M}^{[n]}(\mathbf{X}) = \sum_{I=1}^{NP} \mathbf{H}^{[n]}(\mathbf{X} - \mathbf{X}_I) \mathbf{H}^{[n]T}(\mathbf{X} - \mathbf{X}_I) \Phi_a(\mathbf{X} - \mathbf{X}_I) \quad (49)$$

In (48) the kernel function  $\Phi_a$  is evaluated at the material coordinate. This implies that  $\text{supp}(\Psi_I^{[n]})$  covers the same set of meshfree nodes (attached to material points) under material deformation as shown in Fig. 2.

### Remarks

1. The support of each kernel function must cover sufficient discrete nodes for  $\mathbf{M}^{[n]}$  to be nonsingular. For example, for linear completeness ( $n = 1$ ) in three dimensions, any material point must be covered by at least four noncoplanar shape functions. This is referred to as the kernel stability condition. The kernel stability condition in the Lagrangian reproducing kernel approximation is imposed in the undeformed configuration. This kernel stability is invariant with respect to the material deformation.

## Stress-Strain Computation

In the constitutive equations of multisurface plasticity, Cauchy stress is the primary variable involved in the yield functions, flow rules, and hardening rules. These evolution equations account for the pure deformation of the Cauchy stress increment. Computationally, a strain-driven procedure is used, in that the Cauchy stress increment is obtained from a strain increment by solving a set of evolution equations simultaneously, as shown in Fig. 3. In this stress update, symmetric and

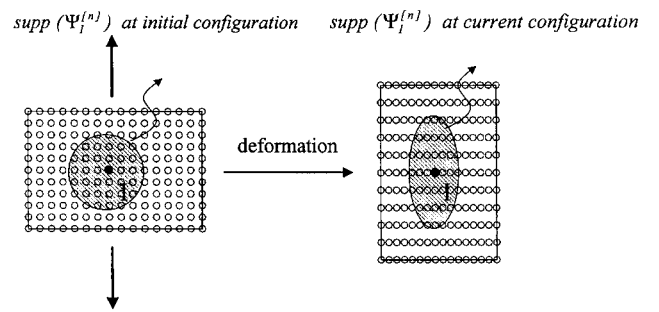


FIG. 2. Kernel Stability of Lagrangian Shape Functions

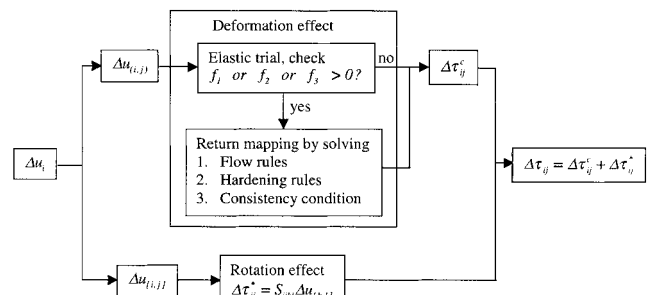


FIG. 3. Stress Update Procedures in Multisurface Plasticity

antisymmetric parts of the displacement spatial gradient are needed. This adds some complication in using the Lagrangian reproducing kernel approximation for plasticity. In Fig. 3,  $\Delta\tau_{ij}^c$  and  $\Delta\tau_{ij}^*$  are associated with the incremental counterparts of the two terms on the right side of (10). The term  $\Delta\tau_{ij}^c$  is the stress increment due to pure deformation, and is obtained from the consistency condition of the yielding functions, the associated flow rules, and the hardening rules [(1)–(7)]. In the incremental procedures, elastic trial and return mapping algorithms are employed. The tangent operator, consistent with the return mapping algorithms, has been proposed by Simo and Taylor (1985). The stress increment  $\Delta\tau_{ij}^*$  is due to rotational effect. The incrementally objective algorithm by Hughes and Winget (1980) has been widely used. A consistent tangent operator consistent to the incrementally objective stress update has recently been proposed by Fish and Shek (1999).

Using the Lagrangian reproducing kernel approximation of displacements in (44),  $\Delta u_{(i,j)}$  is computed as follows:

$$\Delta u_{(i,j)} = \frac{1}{2} \left\{ \frac{\partial}{\partial x_j} \left[ \sum_{l=1}^{NP} \Psi_l^{[n]}(\mathbf{X}) \Delta d_{il}(t) \right] + \frac{\partial}{\partial x_i} \left[ \sum_{l=1}^{NP} \Psi_l^{[n]}(\mathbf{X}) \Delta d_{jl}(t) \right] \right\} \quad (50)$$

$$\Delta u_{(i,j)} = \frac{1}{2} \left\{ \left[ \sum_{l=1}^{NP} \frac{\partial \Psi_l^{[n]}(\mathbf{X})}{\partial X_k} \Delta d_{il}(t) \right] F_{kj}^{-1}(\mathbf{X}, t) + \left[ \sum_{l=1}^{NP} \frac{\partial \Psi_l^{[n]}(\mathbf{X})}{\partial X_k} \Delta d_{jl}(t) \right] F_{ki}^{-1}(\mathbf{X}, t) \right\} \quad (51)$$

A similar method is used to obtain  $\Delta u_{(i,j)}$ . Here  $F_{kj}^{-1} = \partial X_i / \partial x_j$  again requires taking a spatial derivative. Rather than computing  $\mathbf{F}^{-1}$  directly,  $\mathbf{F}$  is first computed by

$$F_{ij} = \delta_{ij} + \frac{\partial u_i}{\partial X_j} = \delta_{ij} + \sum_{l=1}^{NP} \frac{\partial \Psi_l^{[n]}(\mathbf{X})}{\partial X_j} d_{il}(t) \quad (52)$$

where  $\mathbf{F}^{-1}$  is then obtained by inverting  $\mathbf{F}$ . The unknown  $d_{il}(t)$ , however, appears in (52). Numerically, the coefficient  $\Delta d_{il}(t)$  in (50) and (51) is solved from discretization of the weak form of the incremental equilibrium equation at the current time.  $\mathbf{F}$  is computed using  $d_{il}(t)$  at the previous converged load step using (52).

The return mapping procedures and the corresponding co-rotational material response tensor  $C_{ijkl}$  can be found in Wu (1999). These procedures are identical for both meshfree and finite-element computation. It should be noted that for meshfree approximation, higher-order continuous kernel functions are normally employed. For example, the cubic  $B$ -spline kernel function and corresponding meshfree shape functions are  $C^2$  continuous. As a result, stresses and strains can be computed at any point in the domain without the need for averaging or smoothing processes.

### Lagrangian Meshfree Discretization

In the approximation of displacements [48], the Lagrangian shape functions are evaluated using the material coordinate. It is therefore more convenient to transform the weak forms to the initial configuration for discretization as follows:

$$\int_{\Omega_x} \delta u_{i,j} \tau_{ij} d\Omega_x = \int_{\Omega_x} \frac{\partial u_i}{\partial X_k} F_{kj}^{-1} \tau_{ij} J^0 d\Omega_x = \int_{\Omega_x} \frac{\partial u_i}{\partial X_k} \sigma_{ki} d\Omega_x \quad (53)$$

$$\int_{\Omega_x} \delta u_i b_i d\Omega_x = \int_{\Omega_x} \delta u_i b_i J^0 d\Omega_x = \int_{\Omega_x} \delta u_i b_i^0 d\Omega_x \quad (54)$$

$$\begin{aligned} \int_{\Gamma_x^h} \delta u_i h_i d\Gamma_x &= \int_{\Gamma_x^h} \delta u_i \tau_{ij} n_j d\Gamma_x = \int_{\Gamma_x^h} \delta u_i \tau_{ij} N_k F_{kj}^{-1} J^0 d\Gamma_x \\ &= \int_{\Gamma_x^h} \delta u_i \sigma_{ki} N_k d\Gamma_x = \int_{\Gamma_x^h} \delta u_i h_i^0 d\Gamma_x \end{aligned} \quad (55)$$

$$\begin{aligned} \int_{\Omega_x} \delta u_{i,j} (D_{ijkl} + T_{ijkl}) \Delta u_{k,l} d\Omega_x \\ = \int_{\Omega_x} \frac{\partial \delta u_i}{\partial X_m} F_{mj}^{-1} (D_{ijkl} + T_{ijkl}) F_{nl}^{-1} \frac{\partial \Delta u_k}{\partial X_n} J^0 d\Omega_x \end{aligned} \quad (56)$$

where  $J^0 = \det(\mathbf{F})$ ;  $\sigma$  = first Piola-Kirchhoff stress;  $\mathbf{b}^0$  = body force per unit undeformed volume;  $\mathbf{N}$  = surface normal of  $\Gamma_x$ ;  $\mathbf{h}^0$  = surface traction defined as the applied surface force divided by the initial surface area; and  $\mathbf{F}^{-1}$  is obtained from the inversion of  $\mathbf{F}$  by (52). It should be noted that in instances where deformation-dependent surface traction occurs, such as for follower loads,  $\mathbf{h}$  is defined in the current configuration. In this case  $d\Gamma_x = J^0 \|\mathbf{N} \cdot \mathbf{F}\| d\Gamma_x$  is used in (55) without transformation of  $\mathbf{h}$  to  $\mathbf{h}^0$ , with  $\mathbf{h}$  evaluated by  $\mathbf{h}(\mathbf{x}(\mathbf{X}, t))$ .

By introducing Lagrangian meshfree shape functions into the weak form of the equilibrium equation, the meshfree discrete incremental equilibrium equation is obtained

$$\mathbf{K} \Delta \mathbf{d} = \mathbf{f}^{\text{ext}} - \mathbf{f}^{\text{int}} \quad (57)$$

In (57), the stiffness matrix  $\mathbf{K}$ , internal force vector  $\mathbf{f}^{\text{int}}$ , and external force vector  $\mathbf{f}^{\text{ext}}$  are obtained from (56), (53), (54), and (55), respectively, to yield

$$\mathbf{K}_{IJ} = \int_{\Omega_x} \mathbf{B}_I^T (\bar{\mathbf{D}} + \bar{\mathbf{T}}) \mathbf{B}_J d\Omega_x \quad (58)$$

$$\mathbf{B}_I = \begin{bmatrix} \frac{\partial \Psi_I(\mathbf{X})}{\partial X_1} & 0 \\ 0 & \frac{\partial \Psi_I(\mathbf{X})}{\partial X_2} \\ \frac{\partial \Psi_I(\mathbf{X})}{\partial X_2} & 0 \\ 0 & \frac{\partial \Psi_I(\mathbf{X})}{\partial X_1} \end{bmatrix} \quad (59)$$

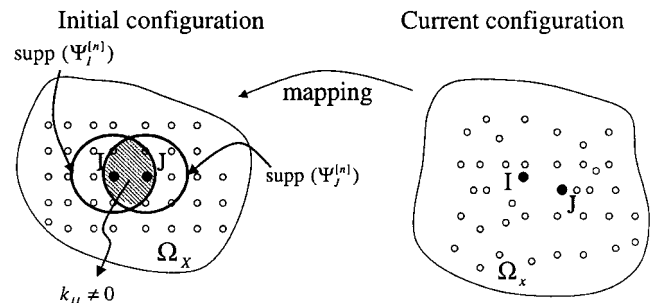


FIG. 4. Integration of  $\mathbf{K}_{IJ}$  in Initial Domain

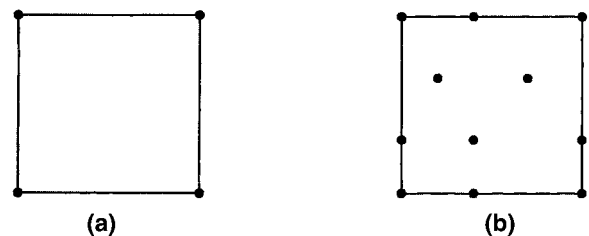


FIG. 5. Meshfree Models for Uniaxial Tension-Compression Test: (a) 4-Node Discretization; (b) Random Discretization

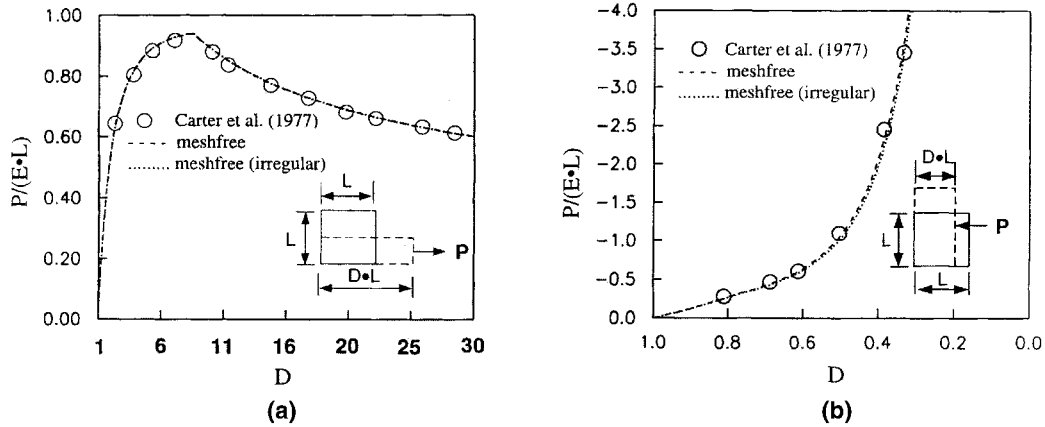


FIG. 6. Comparison of Meshfree and Analytical Solutions in: (a) Tension Test; (b) Compression Test

$$\mathbf{f}_I^{\text{int}} = \int_{\Omega_x} \mathbf{B}_I^T \boldsymbol{\Sigma} d\Omega_x \quad (60)$$

$$\mathbf{f}_I^{\text{ext}} = \int_{\Omega_x} \boldsymbol{\Psi}_I^{[n]} \mathbf{b}^0 d\Omega_x + \int_{\Gamma_x^h} \boldsymbol{\Psi}_I^{[n]} \mathbf{h}^0 d\Gamma_x \quad (61)$$

where  $\mathbf{B}_I$  = gradient matrix associated with node  $I$  constructed based on  $\partial u_i / \partial X_j$ ; and  $\bar{\mathbf{D}}$ ,  $\bar{\mathbf{T}}$ , and  $\boldsymbol{\Sigma}$  are matrix forms of  $J^0 F_{mj}^{-1} D_{ijkl} F_{nl}^{-1}$ ,  $J^0 F_{mj}^{-1} T_{ijkl} F_{nl}^{-1}$ , and first Piola-Kirchhoff stress  $\sigma_{ki} = \tau_{ij} J^0 F_{kj}^{-1}$ , respectively.

#### Remarks

1. The matrix  $\mathbf{K}_{IJ}$  represents the stiffness associated with nodes  $I$  and  $J$ . The gradient matrix  $\mathbf{B}_I$  is nonzero only in  $\text{supp}(\boldsymbol{\Psi}_I^{[n]})$  in the initial domain. Therefore the integration of  $\mathbf{K}_{IJ}$  is only performed in the region  $\text{supp}(\boldsymbol{\Psi}_I^{[n]}) \cap \text{supp}(\boldsymbol{\Psi}_J^{[n]})$  in the initial domain  $\Omega_x$  as shown in Fig. 4. Similarly,  $\mathbf{f}_I^{\text{int}}$  and  $\mathbf{f}_I^{\text{ext}}$  are integrated over  $\text{supp}(\boldsymbol{\Psi}_I^{[n]}) \subset \Omega_x$ .
2. Since  $\boldsymbol{\Psi}_I^{[n]}$  and  $\mathbf{B}_I$  are independent of the material deformation, and the domain and boundary integration is performed over the initial configuration, the values of  $\boldsymbol{\Psi}_I^{[n]}$  and  $\mathbf{B}_I$  at integration points can be stored and reused at every incremental and iteration step.
3. Domain and boundary integration can be performed using Gauss or nodal integration. The employment of Gauss integration requires a set of three- or four-sided background integration zones. The integration zones can be made independent of the node distribution, with the number of integration points determined by the number of nodes located inside an integration zone. It should be noted that a direct nodal integration can be used in meshfree computation due to the use of smooth shape functions. The solution, however, usually suffers from oscillation and has a lower convergence rate. A stabilized conforming nodal integration has recently been proposed (Chen et al. 2001b) to achieve greater computational efficiency without the loss of accuracy in meshfree analysis.
4. Essential boundary conditions cannot be directly imposed in meshfree analysis. A Lagrange multiplier method is often used to impose essential boundary conditions in the weak form (Lu et al. 1994). Another approach is to select the kinematically admissibly test and trial functions in the weak form statement as described in the second section. Two methods have been proposed using this approach (Chen and Wang 2000a): (1) conduct a mixed coordinate transformation

to convert “generalized” displacements associated with the essential boundary to nodal displacements; and (2) introduce singularities to the essential boundary nodes so that the corresponding displacement coefficients  $d_{it}$  at those nodes become nodal values  $u_i^h(\mathbf{X}_I)$  in (44). A recent study by Wagner and Liu (2000) has shown that the collocation method, if done correctly, can converge with a correct rate. Further discussion on the influence of boundary condition treatments on the rate of convergence can be found in Li and Liu (2000).

#### NUMERICAL EXAMPLES

This section presents several numerical examples used to test the proposed meshfree method in geomechanics. To demonstrate the advantage of meshfree methods, some results are compared with finite-element solutions. In the meshfree computation, the Lagrangian meshfree shape function, constructed using a cubic  $B$ -spline kernel function with linear basis, was employed. Unless otherwise specified, a normalized support size (radius of compact support divided by the averaged nodal distance) of 2.0 was employed. The Gauss integration method was used to perform domain integration.

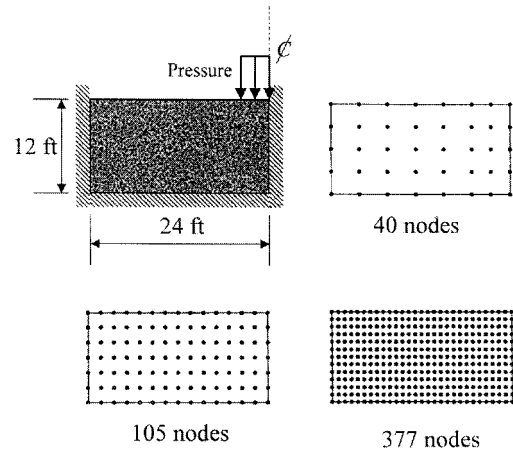


FIG. 7. Analysis Models for Clay Stratum Subjected to Footing Load

TABLE 1. Material Constants for Clay Stratum Footing Loads

Shear failure surface	Coulomb criterion with plane-strain condition	$A$ (psi)	9.22
		$B$	0.112
Elastic parameter	Young's modulus	$E$ (psi)	30,000
	Poisson's ratio	$\nu$	0.3

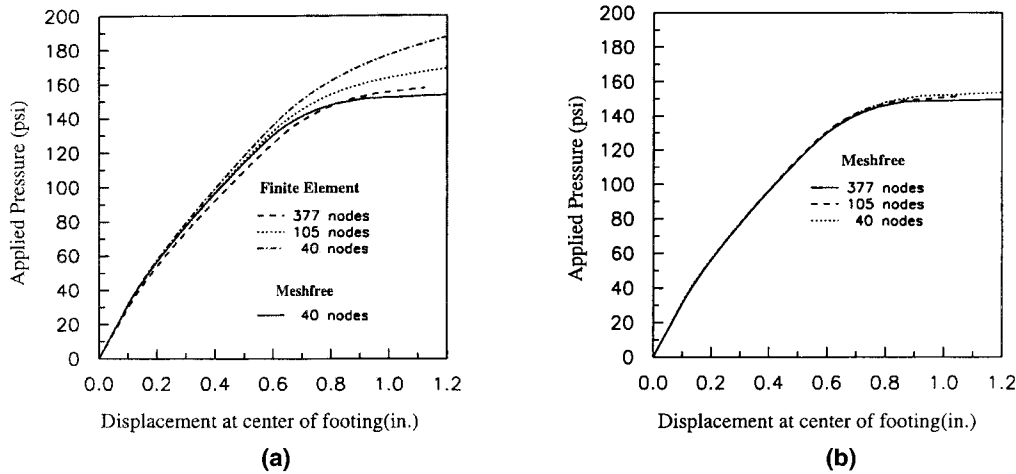


FIG. 8. Comparison of Load-Displacement Solution Using: (a) Finite Element and Meshfree Methods; (b) Meshfree Method

### Uniaxial Tension-Compression

A plane strain homogeneous tension-compression test of an initially stress-free soil was analyzed. For comparison with the finite-strain plasticity analytical solution given by Carter et al. (1977), only the Drucker-Prager yield surface with perfect plasticity was considered in this study. The elastic response was assumed to be linear, with Young's modulus  $E = 30$  MPa and Poisson's ratio 0.3. Carter et al. (1977) assumed a cohesion twice that of Young's modulus for the extension test and 10% of Young's modulus for compression. The material properties for the Drucker-Prager yield surface used in (1) and (2) are

In tension

$$A = 70.602 \text{ MPa}, \quad B = 0.226455405$$

In compression

$$A = 3.531 \text{ MPa}, \quad B = 0.226455405$$

Uniaxial tension and compression deformation of a soil sample was introduced by specifying appropriate displacement boundary conditions that allowed free contraction in the lateral direction. A four-node discretization [Fig. 5(a)] and a random discretization [Fig. 5(b)] were used in the meshfree computation to model one-fourth of a square domain. The results for the tension and compression tests are shown in Figs. 6(a and b), respectively. In both cases, the meshfree solution agreed well with the analytical solution.

### Clay Stratum Subjected to Footing Load

The objective of this analysis was to study the convergence of the meshfree method, and to compare solution accuracy between finite element and the proposed meshfree method. The elastic-plastic response of a clay stratum subjected to a footing load has been investigated by Mizuno and Chen (1983). In this example, three different model refinements for finite element and meshfree methods were employed to analyze the load-displacement response using the Drucker-Prager yield criterion. The material constants obtained by matching the Drucker-Prager model with the Coulomb model using plane strain conditions (Mizuno and Chen 1980) are used in the analysis. Boundary conditions, geometry, and three model refinements used in the analysis are illustrated in Fig. 7. Note that the materials are free to slide on the cutoff boundaries. The material constants used are listed in Table 1. In the finite-element analysis, a four-node bilinear element formulation was employed, whereas linear basis functions were used for the meshfree approximation.

Fig. 8(a) shows the load-displacement curves predicted by the finite-element method using three different mesh refinements and the meshfree method using the coarse model. A stiffer response is observed in the finite-element solution using the coarse meshes. The meshfree method with a coarse 40-node model is capable of yielding a solution of similar accuracy to that of a 377-node finite-element solution. The convergence of the meshfree solution is shown in Fig. 8(b).

### Vertical Cut

The behavior of sand under a vertical cut was studied using both finite element and meshfree methods. A  $12 \times 12$  ft vertical slope earth is subjected to a 4 ft-wide strip footing load. The footing is assumed to be rigid and perfectly rough. Four meshfree models and associated boundary conditions are shown in Fig. 9. Note that the materials are free to slide on the cutoff boundaries. In this example, the Drucker-Prager model, as well as the soil-cap model, were considered in the analysis. The material properties from the previous subsection were used in the Drucker-Prager model. The material constants for the soil-cap model are listed in Table 2 (Mizuno and Chen 1980).

The first three discrete models shown in Fig. 9 were gen-

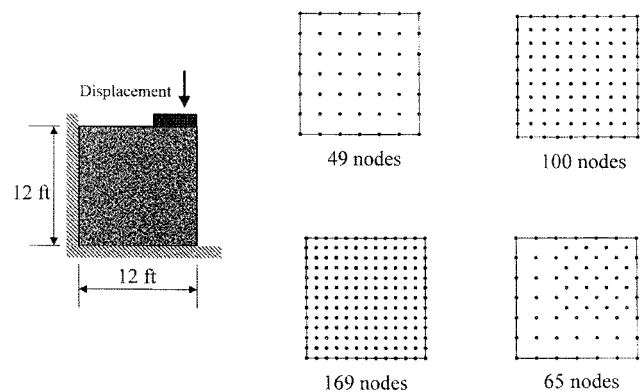


FIG. 9. Analysis Models for Vertical Cut Analysis

TABLE 2. Material Constants for Soil-Cap Model (Mizuno and Chen 1983)

Cap yield surface	Aspect ratio of elliptic	$R$	4.0
Cap hardening	Hardening parameter	$W$	0.003
	Hardening parameter	$\alpha$ (ft <sup>2</sup> /lb)	$6.042e^{-5}$
	Initial cap	$Y_0$ (psi)	46.53
Tension cutoff surface	Maximum allowable hydrostatic tension	$T$ (psi)	0.0

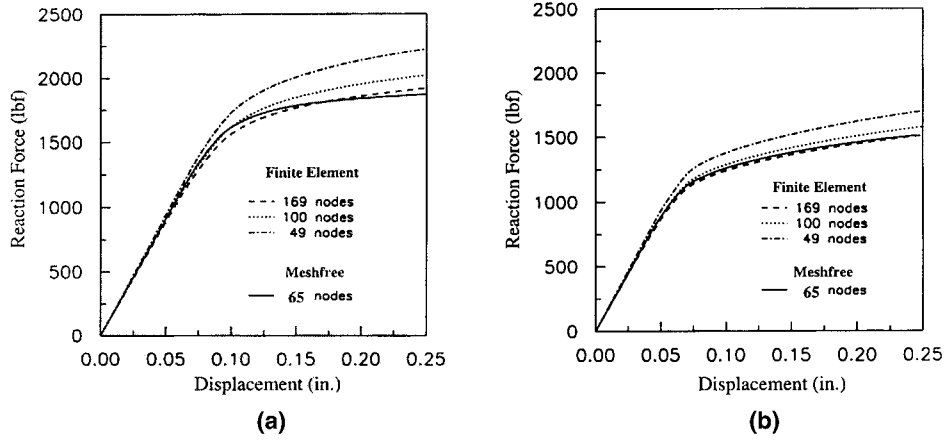


FIG. 10. Comparison of Load-Displacement Responses Using: (a) Drucker-Prager Model; (b) Soil-Cap Model

erated using a uniform refinement for the finite-element analysis, where every four nodes were connected to form a 4-node bilinear element. The fourth model in Fig. 9 is a meshfree adaptive model created by inserting one node into the centroid of every 4-node zone in the coarse finite-element model. Given the conforming property of meshfree shape functions and without the burden of a mesh, an h-type adaptivity can be performed with greater simplicity using the meshfree method.

The load-displacement curves of a Drucker-Prager model obtained from both finite element and meshfree methods are shown in Fig. 10(a). Similar analyses, performed using the soil-cap model, are compared in Fig. 10(b). As can be seen from Fig. 10, a meshfree solution with 65-node discretization converges to results almost identical to that of the refined 169-node finite-element analysis. Fig. 10 also shows that the load-displacement curve predicted by the soil-cap model reaches yielding earlier than that of the Drucker-Prager yielding criterion. This is due to the fact that the Drucker-Prager yield function neglects the influence of compressive volumetric plastic deformation.

## CONCLUSIONS

An implementation of meshfree method for analysis of geotechnical materials is presented. The Lagrangian description of material behavior in the strong and weak forms is employed as the basis of Galerkin meshfree approximation. To simulate material deformation by following fixed material particles, a Lagrangian reproducing kernel approximation is introduced to construct the Lagrangian meshfree shape functions. The reproducing conditions are imposed at the material coordinate to achieve a desired completeness of the approximation. The resulting meshfree shape functions are therefore independent of material deformation. Kernel stability is also determined by the nodal locations in the undeformed domain. To construct meshfree discrete equations using the Lagrangian shape functions, the weak forms are transformed to the undeformed domain.

The evolution equations of geotechnical materials involve Cauchy stress that needs to be updated using spatial derivatives of displacement increments referenced to the current configuration. A chain rule is employed so that the spatial derivatives are replaced by the multiplication of material derivatives and the inversion of the deformation gradient. The calculation of the deformation gradient can be easily performed using the material derivatives of the Lagrangian meshfree shape functions. In this study, multisurface plasticity with cap hardening is used as a model problem for meshfree analysis of geotechnical materials.

Three benchmark problems are analyzed to evaluate the per-

formance of meshfree methods for geotechnical applications. The numerical results demonstrate that the proposed meshfree method with linear basis functions provides higher solution accuracy than the classical bilinear finite-element method. The third example also demonstrates that by using the conforming property of meshfree shape functions, an h-type adaptivity can be easily implemented with a direct node insertion in the meshfree discretization.

Although good solution accuracy has been demonstrated in this study, the high computational cost and the use of an “integration cell” for Gauss integration present the major bottlenecks in applying the meshfree method. The use of a higher-order quadrature rule in the Gauss integration of the weak form consumes considerable CPU, and the large bandwidth in the meshfree stiffness matrix adds additional complexity to the solution procedure of meshfree methods. The recent work by Chen et al. (2001b) introduced a stabilized conformation nodal integration for Galerkin meshfree methods to significantly reduce the computational effort in the formation of stiffness matrix and force vectors, without sacrificing accuracy. In the next stage of this study, the stabilized conforming nodal integration will be further extended to geotechnical materials to partially resolve the aforementioned disadvantages in the present method.

## APPENDIX. TANGENT MODULUS OF SOIL-CAP MODEL

The notations used in this section follow those defined in Fig. 1 and the second section. By following the procedures presented in Simo et al. (1988b), the tangent modulus for different modes of the soil-cap model can be obtained as follows (Wu 2000):

1. Shear failure mode: Active when  $f_{1,n+1}^{\text{trial}} > 0$ ,  $\Delta\gamma_{1,n+1} > 0$ , and  $\Delta\gamma_{2,n+1} = \Delta\gamma_{3,n+1} = 0$ . Similar to single-surface plasticity, the tangent modulus can be expressed explicitly by

$$\mathbf{C}_{n+1} = \mathbf{C}^e - \frac{(3K\mathbf{I} + 2G\mathbf{n}_{n+1}) \otimes (3K\mathbf{I} + 2G\mathbf{n}_{n+1})}{2G + 9KB^2} - \frac{4G^2}{\|\boldsymbol{\tau}_{n+1}^{\text{trial}}\|} [\mathbf{I}_{\text{dev}} - \mathbf{n}_{n+1} \otimes \mathbf{n}_{n+1}] \Delta\gamma_{1,n+1} \quad (62)$$

where  $\mathbf{C}^e$  = elasticity tensor;  $G$  = shear modulus;  $K$  = bulk modulus;  $\mathbf{I}$  = fourth-order symmetric unit tensor;  $\mathbf{I}_{\text{dev}}$  = deviator of  $\mathbf{I}$ ,  $(\cdot)_{n+1}$  = value of a variable  $(\cdot)$  at the end of a typical time step  $[t_n, t_{n+1}]$ ;  $\mathbf{n}_{n+1}$  = unit vector field normal to the yield surface; and  $\Delta\gamma_{1,n+1}$  = discrete

consistency parameter with respect to shear failure surface.

2. Tension cutoff mode: Active when  $f_{2,n+1}^{\text{trial}} > 0$ ,  $\Delta\gamma_{2,n+1} > 0$ , and  $\Delta\gamma_{1,n+1} = \Delta\gamma_{3,n+1} = 0$ . Due to the fact that perfect plastic behavior is assumed in the tension cutoff surface, the tangent modulus can be simplified as

$$C_{n+1} = 2G\mathbf{I}_{\text{dev}} \quad (63)$$

3. Tension corner mode: Active when  $\Delta\gamma_{1,n+1} > 0$ ,  $\Delta\gamma_{2,n+1} > 0$ , and  $\Delta\gamma_{3,n+1} = 0$ . Following the discrete version of Koiter's generalized flow rule [(7)], the tangent modulus can be obtained as

$$C_{n+1} = -\frac{4G^2}{\|\boldsymbol{\tau}_{n+1}^{\text{trial}}\|} [\mathbf{I}_{\text{dev}} - \mathbf{n}_{n+1} \otimes \mathbf{n}_{n+1}] \Delta\gamma_{1,n+1} \quad (64)$$

4. Ellipsoidal cap mode: Active when  $f_{3,n+1}^{\text{trial}} > 0$ ,  $\Delta\gamma_{3,n+1} > 0$ , and  $\Delta\gamma_{1,n+1} = \Delta\gamma_{2,n+1} = 0$ . The derivation of the tangent modulus in the cap mode is performed using the same strategy as that in the other modes, except that the hardening rule is no longer associative

$$\begin{aligned} C_{n+1} = & \mathbf{C}^e - \left[ \frac{6(I_{1,n+1} - k_{n+1})}{R^2} \mathbf{1} + 4G\|\boldsymbol{\tau}_{n+1}^d\| \mathbf{n}_{n+1} \right] \\ & \otimes \frac{d\Delta\gamma_{3,n+1}}{d\boldsymbol{\epsilon}_{n+1}} - \Delta\gamma_{3,n+1} \left[ \frac{6}{R^2} \mathbf{1} \otimes \left( \frac{d\Delta\gamma_{3,n+1}}{d\boldsymbol{\epsilon}_{n+1}} - \frac{dk_{n+1}}{d\boldsymbol{\epsilon}_{n+1}} \right) \right. \\ & \left. + 4G\mathbf{n}_{n+1} \otimes \frac{d\|\boldsymbol{\tau}_{n+1}^d\|}{d\boldsymbol{\epsilon}_{n+1}} \right] + 4G\|\boldsymbol{\tau}_{n+1}^d\| \frac{d\mathbf{n}_{n+1}}{d\boldsymbol{\epsilon}_{n+1}} \end{aligned} \quad (65)$$

where

$$\begin{aligned} \frac{dk_{n+1}}{d\boldsymbol{\epsilon}_{n+1}} &= \frac{3Ka_{13}\mathbf{1} + a_{12} \frac{d\Delta\gamma_{3,n+1}}{d\boldsymbol{\epsilon}_{n+1}}}{a_{11} + a_{13}b_{11}} \\ \frac{dI_{1,n+1}}{d\boldsymbol{\epsilon}_{n+1}} &= 3K\mathbf{1} - b_{11} \frac{dk_{n+1}}{d\boldsymbol{\epsilon}_{n+1}} \\ \frac{d\Delta\gamma_{3,n+1}}{d\boldsymbol{\epsilon}_{n+1}} &= \frac{c_{11}}{c_{12}} \\ \frac{d\|\boldsymbol{\tau}_{n+1}^d\|}{d\boldsymbol{\epsilon}_{n+1}} &= \|\boldsymbol{\tau}_{n+1}^d\| \left[ \frac{2G\mathbf{n}_{n+1}}{1 + 4G\Delta\gamma_{3,n+1}} - \frac{4G\|\boldsymbol{\tau}_{n+1}^d\|}{1 + 4G\Delta\gamma_{3,n+1}} \frac{d\Delta\gamma_{3,n+1}}{d\boldsymbol{\epsilon}_{n+1}} \right] \end{aligned} \quad (66)$$

and

$$\begin{aligned} a_{11} &= 1 + \frac{6\Delta\gamma_{3,n+1}}{\bar{h}R^2} \\ a_{12} &= \frac{6(I_{1,n+1} - k_{n+1})}{\bar{h}R^2} \\ a_{13} &= \frac{6\Delta\gamma_{3,n+1}}{\bar{h}R^2} \\ \bar{h} &= W\alpha(1 + RB)e^{-\alpha Y(k_{n+1})} \\ b_{11} &= 3K\bar{h} \\ c_{11} &= \left[ \frac{6(I_{1,n+1} - k_{n+1})}{R^2} \frac{1}{a_{11} + a_{13}b_{11}} - \frac{12F_e(k_{n+1})BK a_{13}}{a_{11} + a_{13}b_{11}} \right] \mathbf{1} \\ &+ \frac{4G\|\boldsymbol{\tau}_{n+1}^d\|}{1 + 4G\Delta\gamma_{3,n+1}} \mathbf{n}_{n+1} \\ c_{12} &= 36K \left[ \frac{I_{1,n+1} - k_{n+1}}{R^2} \right]^2 \left[ \frac{1}{a_{11} + a_{13}b_{11}} \right] + \frac{8G\|\boldsymbol{\tau}_{n+1}^d\|^2}{1 + 4G\Delta\gamma_{3,n+1}} \end{aligned} \quad (67)$$

$$+ 12 \left[ \frac{I_{1,n+1} - k_{n+1}}{R^2} + F_e(k_{n+1})B \right] \frac{I_{1,n+1} - k_{n+1}}{\bar{h}R^2} \frac{1}{a_{11} + a_{13}b_{11}} \quad (68)$$

where  $R$ ,  $W$ ,  $Y$ ,  $\alpha$ , and  $k$  = material parameters defined in the second section. It is noted that this tangent modulus is not symmetric. The reason for this asymmetry is that the soil-cap model does not obey the principle of maximum plastic dissipation.

5. Compressive corner mode: Active when  $\Delta\gamma_{1,n+1} > 0$ ,  $\Delta\gamma_{3,n+1} > 0$ , and  $\Delta\gamma_{2,n+1} = 0$ . From the hardening law it follows that the shear failure surface and the ellipsoidal cap behave as perfect plasticity. The tangent modulus can be carried out similar to the tension corner region by enforcing Koiter's generalization

$$\begin{aligned} C_{n+1} = & -(4G\|\boldsymbol{\tau}_{n+1}^d\| \Delta\gamma_{3,n+1} + 2G\Delta\gamma_{1,n+1}) \\ & \cdot \left( \frac{2G}{\|\boldsymbol{\tau}_{n+1}^d\|} [\mathbf{I}_{\text{dev}} - \mathbf{n}_{n+1} \otimes \mathbf{n}_{n+1}] \right) \end{aligned} \quad (69)$$

## ACKNOWLEDGMENT

The support of this research by Caterpillar, Inc., to the University of Iowa is greatly acknowledged.

## REFERENCES

- Atluri, S. N., and Zhu, T. (1998). "A new meshless local Petrov-Galerkin (MLPG) approach." *Computational Mech.*, 22, 117–127.
- Babuska, I., and Melenk, J. M. (1997). "The partition of unity method." *Int. J. Numer. Methods in Engrg.*, 40, 727–758.
- Beissel, S., and Belytschko, T. (1996). "Nodal integration of the element-free Galerkin method." *Comput. Methods Appl. Mech. Engrg.*, 139, 49–74.
- Belytschko, T., Kronggauz, Y., Organ, D., and Fleming, M. (1996). "Meshless methods: An overview and recent developments." *Comput. Methods Appl. Mech. Engrg.*, 139, 3–47.
- Belytschko, T., Lu, Y. Y., and Gu, L. (1994). "Element-free Galerkin methods." *Int. J. Numer. Methods in Engrg.*, 37, 229–256.
- Carter, J. P., Booker, J. R., and Davis, E. H. (1997). "Finite deformation of an elastoplastic soil." *Int. J. Numer. and Analytical Methods in Geomech.*, 1, 25–43.
- Chen, W. F., and Baladi, G. Y. (1985). *Soil plasticity: Theory and implementation*, Elsevier Science Publishing Co., Inc., New York.
- Chen, J. S., Pan, C., Roque, C., and Wang, H. P. (1998). "A Lagrangian reproducing kernel particle method for metal forming analysis." *Computational Mech.*, 22, 289–307.
- Chen, J. S., Pan, C., Wu, C. T., and Liu, W. K. (1996). "Reproducing kernel particle methods for large deformation analysis of nonlinear structures." *Comput. Methods Appl. Mech. Engrg.*, 139, 195–227.
- Chen, J. S., and Wang, H. P. (2001a). "New boundary condition treatments for meshless computation of contact problems." *Comput. Methods Appl. Mech. Engrg.*, 187, 441–468.
- Chen, J. S., Wu, C. T., Yoon, S., and You, Y. (2001b). "A stabilized conforming nodal integration for Galerkin meshfree methods." *Int. J. Numer. Methods in Engrg.*, 50, 435–466.
- DiMaggio, F. L., and Sandler, I. S. (1971). "Material model for granular soils." *J. Engrg. Mech.*, ASCE, 97, 935–950.
- Duarte, C. A., and Oden, J. T. (1996). "H-p clouds: An h-p meshless method." *Numer. Methods Partial Differential Equations*, 12, 673–705.
- Fish, J., and Shek, K. (1999). "Computational aspects of incrementally objective algorithms for large deformations plasticity." *Int. J. Numer. Methods in Engrg.*, 44, 839–851.
- Hofstetter, G., Simo, J. C., and Taylor, R. L. (1993). "A modified cap model: Closet point solution algorithms." *Comp. and Struct.*, 46, 203–214.
- Hughes, T. J. R., and Winget, J. M. (1980). "Finite rotation effects in numerical integration of rate constitutive equations arising in large deformation analysis." *Int. J. Numer. Methods in Engrg.*, 16, 1862–1867.
- Kaljevic, I., and Saigal, S. (1997). "An improved element-free Galerkin formulation." *Int. J. Numer. Methods in Engrg.*, 40, 2953–2974.
- Koiter, W. T. (1953). "Stress-strain relations, uniqueness, and variational theorems for elastic-plastic materials with a singular yield surface." *Quarterly J. Appl. Math.*, 11, 350–354.
- Lancaster, P., and Salkauskas, K. (1981). "Surfaces generated by moving least-squares methods." *Math. Computation*, 37, 141–158.

- Li, S., and Liu, W. K. (2000). "Numerical simulation of strain localization in inelastic solids using meshfree methods." *Int. J. Numer. Methods in Engrg.*, 48, 1295–1309.
- Liu, W. K., Jun, S., Li, S., Adee, J., and Belytschko, B. (1995a). "Reproducing kernel particle methods for structural dynamics." *Int. J. Numer. Methods in Engrg.*, 38, 1655–1679.
- Liu, W. K., Jun, S., and Zhang, Y. F. (1995b). "Reproducing kernel particle methods." *Int. J. Numer. Methods in Fluids*, 20, 1081–1106.
- Lu, Y. Y., Belytschko, T., and Gu, L. (1994). "A new implementation of the element-free Galerkin method." *Comput. Methods Appl. Mech. Engrg.*, 113, 397–414.
- Melenk, J. M., and Babuska, I. (1996). "The partition of unity finite-element method: Basic theory and applications." *Comput. Methods Appl. Mech. Engrg.*, 139, 289–314.
- Mizuno, E., and Chen, W. F. (1980). "Analysis of soil response with different plasticity models." *Proc., Symp. on Limit Equilibrium, Plasticity, and Generalized Stress-Strain Applications in Geotech. Engrg.*, 115–138.
- Mizuno, E., and Chen, W. F. (1983). "Cap models for clay strata to footing loads." *Comp. and Struct.*, 17, 511–528.
- Monaghan, J. J. (1988). "An introduction to SPH." *Comp. Phys. Communications*, 48, 89–96.
- Nayroles, B., Touzot, G., and Villon, P. (1992). "Generalizing the finite-element method: Diffuse approximation and diffuse elements." *Computational Mech.*, 10, 307–318.
- Randles, P. W., and Libersky, L. D. (1996). "Smoothed particle hydrodynamics: Some recent improvements and applications." *Comput. Methods Appl. Mech. Engrg.*, 139, 275–408.
- Sandler, I. S., and Rubin, D. (1979). "An algorithm and a modular subroutine for the cap model." *Int. J. Numer. and Analytical Methods in Geomech.*, 3, 173–186.
- Simo, J. C., Ju, J. W., Pister, K. S., and Taylor, R. L. (1988a). "Assessment of cap model: Consistent return algorithms and rate-dependent extension." *J. Engrg. Mech.*, ASCE, 114, 191–218.
- Simo, J. C., Kennedy, J. G., and Govindjee, S. (1988b). "Nonsmooth multisurface plasticity and viscoplasticity—Loading-unloading conditions and numerical algorithms." *Int. J. Numer. Methods in Engrg.*, 26, 2161–2185.
- Simo, J. C., and Taylor, R. L. (1985). "Consistent tangent operators for rate-independent elastoplasticity." *Comput. Methods Appl. Mech. Engrg.*, 48, 101–118.
- Sulsky, D., Chen, Z., and Schreyer, H. L. (1994). "A material point method for history-dependent materials." *Comput. Methods Appl. Mech. Engrg.*, 118, 179–196.
- Wagner, G. J., and Liu, W. K. (2000). "Application of essential boundary conditions in meshfree methods: A corrected collocation method." *Int. J. Numer. Methods in Engrg.*, 47, 1367–1379.
- Wu, C. T. (1999). "Reproducing kernel formulation for multisurface plasticity and continuum damage mechanics in geotechnical materials." PhD thesis, University of Iowa, Iowa City, Iowa.